THEORETICAL INVESTIGATION OF THERMOELECTRIC PROPERTIES OF BULK AND NANO-SCALED SEMICONDUCTORS

BY

KYEONG HYUN PARK

THESIS

Submitted in partial fulfillment of the requirements
for the degree of Master of Science in Electrical and Computer Engineering
in the Graduate College of the
University of Illinois at Urbana-Champaign, 2012

Urbana, Illinois

Adviser:

Professor Umberto Ravaioli

Abstract

Even though thermoelectric effects have drawn more attention these days due to environmental and economic reasons, the efficiency of the thermoelectric technology is still limited by currently available thermoelectric materials. The priority aim in thermoelectric industry is to achieve a higher ZT, the dimensionless thermoelectric figure of merit. There are key thermoelectric properties determining the efficiency ZT: Seebeck coefficient, electrical conductivity, and thermal conductivity. This work mainly focuses on strategies to obtain higher ZT and will walk through each thermoelectric property calculation for bulk and nano-scaled semiconductors using Landauer and phonon Boltzmann transport approaches. As a reduction of thermal conductivity in nanoscale semiconductor wires has been reported for the last decade, scaling of semiconductor devices changes the way heat flows through a system due to a significant increase in boundary scattering. It will be well shown that the thermal conductivity of nanoscale semiconductors significantly decreases compared to that of bulk semiconductors. Considering an enhancement of ZT, a decrease in thermal conductivity is a significant issue in designing new devices while retaining electrical conductivity. Therefore, at the end, geometrically engineered semiconductor nanowires and superlattice nanowires will be investigated to show even more reduced phononic transport properties compared to the straight and pure semiconductor nanowires. These results will be expected to suggest prospective ideas to improve the current thermoelectric technology.

Contents

1. Introduction

1.1 Thermoelectric Devices

Thermoelectric devices have recently captured a lot of interest in the scientific community as a viable resource for power generation through converting waste thermal energy into electricity or cooling systems. What makes thermoelectric devices superior to existing energy conversion devices is the fact that they do not have any moving parts or fluids, so they are more environmentally friendly and energy-efficient. For instance, conventional refrigerators pollute the atmosphere due to leaking chlorofluorocarbons (CFCs) and have problems with mechanical failure of moving parts. While current thermoelectric devices are focused on converting electricity into heating or cooling energy, generating electricity out of wasted heat energy is getting much more attention as the world is gradually running short of natural resources.

The efficiency of a thermoelectric system is measured through a dimensionless quantity referred to as the thermoelectric figure of merit, which is the product of the Carnot efficiency and a materials conversion efficiency factor: $ZT = S^2\sigma T/\kappa$ [1]. S is the Seebeck coefficient, σ is electrical conductivity, T is the absolute temperature, and κ is thermal conductivity. The higher the ZT, the more adequately electricity is generated out of the material. As the expression of ZT indicates, a material with higher electrical transport properties and a lower thermal transport property is desired to enhance the thermoelectric figure of merit. In this regard, silicon nanowire is among the best candidates for thermoelectric applications due to the large difference in mean free path between electrons and phonons at room temperature, the upshot of this being a reduced thermal conductivity without affecting other electrical properties [2].

1.2 Thermoelectric Effects

There are three key thermoelectric effects: the Seebeck effect, the Peltier effect, and the Thomson effect. The Seebeck effect named for Thomas Johann Seebeck in 1821 [3], is the only effect concerning generation of electricity as a result of a temperature gradient in thermocouples. When heat is applied on one side of the semiconductor instead of holding it at a constant temperature, the temperature difference forms and a certain voltage develops along the semiconductor. This voltage is called the Seebeck voltage. Just as a current is proportional to the applied voltage in a linear transport system with near-equilibrium condition, the voltage that develops is expected to be proportional to the small temperature difference and the constant of the proportionality is called the Seebeck coefficient.

While the Seebeck effect concerns electric fields produced by temperature gradients, the Peltier effect describes the evolution or absorption of heat caused by the flow of electric current [4]. If a positive current flows through a resistor, electrons that have random thermal motions will flow in the opposite direction to the current and carry heat along with them since each electron has a non-degenerate kinetic energy. As a result, the contact from which electrons carry heat away gets cold, and the other side gets hot since the electrons dissipate the heat when they come out. This effect is called Peltier heating or Peltier cooling [5].

2. Thermoelectric Transport Properties of Semiconductors

2.1 Boltzmann Transport Equation

The thermoelectric properties mentioned above are usually obtained by solving the Boltzmann transport equation (BTE) which is a semi-classical approach to carrier transport. The main purpose of solving the Boltzmann equation is to find the electrical and thermal currents which are linear functions of the electric field and temperature gradients [6].

$$J = L_{EE}E + L_{ET}\nabla T \quad (1)$$

$$U = L_{TE}E + L_{TT}\nabla T \quad (2)$$

The first subscripted letter of the coefficients L_{EE}, L_{ET}, L_{TE}, and L_{TT} indicates which current it contributes to and the second letter tells which source it takes into account between the electric field and the temperature gradients. Instead of observing these coefficients directly, two arrangements of the apparatus enable measuring the electrical and thermal properties. In the first setup an electric field is applied with constant temperature along the apparatus and determines the electrical conductivity, $\sigma = L_{EE}$. In the second arrangement an open circuit prevents electric current from flowing through the apparatus and the temperature gradient is maintained. Setting $J = 0$, it gives a relation between E and ∇T, and the thermal conductivity κ, $U = -\kappa\nabla T$, is defined as $\kappa = -\left(L_{TT} - \frac{L_{TE} \cdot L_{ET}}{L_{EE}}\right)$. Although no electrical current flows, an electric field builds up along the device to stop the electric current flow derived by the heat flux, and this electric field slightly reduces the thermal current [6]. The induced electric field subject to a thermal gradient is simply expressed as $E = Q\nabla T$, and the thermopower, which is often called the Seebeck coefficient, is $S = -L_{ET}/L_{EE}$. The coefficients are defined by combining the electric

current density, the heat current density, and the solution to the BTE, and they are as follows [6]: $L_{EE} = e^2\varkappa_0$, $L_{ET} = -e\varkappa_1/T = L_{TE}$, and $L_{TT} = -\varkappa_2/T$, where

$$\varkappa_n = -\frac{1}{3}\int \mathrm{v_k}^2\,\tau(k)(\mathcal{E}_k - \zeta)^n \frac{\partial f_k^0}{\partial \mathcal{E}_k}\mathrm{dk} \tag{3}$$

2.2 Landauer Formalism

2.2.1 Landauer formula

For a given voltage across its ends, a 1D channel has a finite capacity for current flow for a given voltage across its ends. Consider that only one subband is occupied within a wire connecting two larger reservoirs with a certain voltage difference as shown in Fig. 1. The current flowing through the channel becomes [7]

$$I = \Delta nqv = \frac{\rho_1 qV}{L}qv = \frac{2}{hv}vq^2V = \frac{2q^2}{h}V \tag{4}$$

where ρ_1 is the density of states of moving carriers in reservoir 1. This relation implies that in 1D a current depends only on the voltages and the constants by cancelling out the velocity term with the density of states, and it produces the quantized conductance through the channel, $I/V = G_0 = 2q^2/h$. While this quantum conductance is valid when no scattering occurs in a wire, the overall conductance with scattering effect is the quantum of conductance times the probability of electron transmission through the channel $\mathfrak{I}(\mathcal{E})$ [8]

$$G = (2q^2/h)\mathfrak{I}(\mathcal{E}). \tag{5}$$

This equation is called the Landauer formula. For multiple channels, the total transmission probability becomes the sum of the probabilities over the channels that contribute to electron

transmission, $\Im(\mathcal{E}) = \sum_{i,j} \Im(\mathcal{E})$, where i, j label the transverse eigenstates. In addition to the multiple channels, the net current should take into account finite temperature or voltage differences applied to the wire by multiplying the variation of Fermi-Dirac distributions of the electrons in the left and the right, integrated over all energies.

$$I(\mathcal{E}) = \frac{2q}{h} \int_{-\infty}^{\infty} d\mathcal{E}[f_1 - f_2]\Im(\mathcal{E}) \tag{6}$$

When both voltage and temperature differences are applied to the system, a difference of the Fermi distributions over all the energy levels can be simply expressed by the superposition sum of each of the two cases.

$$f_1 - f_2 \approx \left(-\frac{\partial f_0}{\partial \mathcal{E}}\right) q\Delta V - \left(-\frac{\partial f_0}{\partial \mathcal{E}}\right) \frac{(\mathcal{E} - \mathcal{E}_F)}{T} \Delta T \tag{7}$$

2.2.2 Thermoelectric properties

Thermoelectric properties can be evaluated using the Landauer approach, and it is more effective for low temperature applied to mesoscopic structures. In the same manner as the current density equations (Eqs. (1) and (2)), current equations with the Landauer formalism in the linear response regime can be expressed as a combination of electric potential and temperature contributions with electrical transport properties [4],

$$I(\mathcal{E}) = G(\mathcal{E})\Delta V - [SG(\mathcal{E})]\Delta T \tag{8}$$

$$I_q(\mathcal{E}) = -T[SG(\mathcal{E})]\Delta V - \kappa_0 \Delta T \tag{9}$$

Plugging in Eq. (7) into Eq. (6) gives the same form as Eq. (8) with the voltage and temperature terms, and a comparison of these equations defines the electrical conductance, the Seebeck coefficient, and the thermal conductance for zero electric current as [9]

$$G(\mathcal{E}) = \frac{2q^2}{h}\int_{-\infty}^{\infty}\Im(\mathcal{E})\left(-\frac{\partial f_0}{\partial \mathcal{E}}\right)d\mathcal{E} \quad (1/\Omega) \tag{10}$$

$$S(\mathcal{E}) = \left(\frac{k_B}{-q}\right)\frac{\int_{-\infty}^{\infty}\Im(\mathcal{E})[(\mathcal{E}-\mathcal{E}_F)/k_BT]\left(-\frac{\partial f_0}{\partial \mathcal{E}}\right)d\mathcal{E}}{\int_{-\infty}^{\infty}\Im(\mathcal{E})\left(-\frac{\partial f_0}{\partial \mathcal{E}}\right)d\mathcal{E}} \quad (V/\mathrm{K}) \tag{11}$$

$$\kappa_0 = \frac{2}{hT}\int_{-\infty}^{\infty}\Im(\mathcal{E})(\mathcal{E}-\mathcal{E}_F)^2\left(-\frac{\partial f_0}{\partial \mathcal{E}}\right)d\mathcal{E} \quad (W/\mathrm{K}) \tag{12}$$

where $S = [SG]/G$ and $\kappa_e = \kappa_0 - TS^2G$ [10].

2.2.3 Transmission function

The transmission function $\Im(\mathcal{E})$, which is an essential property that defines the current (Eq. (6)) through a conductor as well as the thermoelectric properties, is composed of the transmission probability and the number of conducting channels, $\Im(\mathcal{E}) = T(\mathcal{E})M(\mathcal{E})$. The transmission probability $T(\mathcal{E})$ is the probability of transmission taking reflections into account. Consider that two conductors are connected in series with transmission probability T_1 and T_2. See Fig. 2(a). The total transmission cannot be simply the product of the two probabilities since multiple transmissions from the back and forth reflections must be included [11]. Therefore, the transmission probability is obtained by summing the probabilities of all the multiply reflected paths as well as the direct transmissions as shown in Fig. 2(b). The total transmission probability can be simplified using an infinite geometric expansion of the Maclaurin series since each of both transmission and reflection probabilities is less than unity, and therefore

$$T_{12} = T_1T_2 + T_1T_2R_1R_2 + T_1T_2R_1^2R_2^2 + \cdots = \frac{T_1T_2}{1-R_1R_2} \tag{13}$$

Using a property $T = 1 - R$, the transmission property with N conductors connected in series, each having the same transmission probability, is given by $T(N) = T/(N(1-T)+T)$, and the

final expression becomes $T(L) = \frac{\Lambda}{L+\Lambda}$, where L is the length of a conductor and Λ is the mean free path, the average distance an electron can travel before it is scattered [11].

The number of conducting channels $M(\mathcal{E})$, also known as density of modes, defines the maximum conductance by counting conducting channels through which carriers transport with the transmission probability $T(\mathcal{E})$ [8]. A conductance with a finite cross section is ready to be computed by obtaining the density of modes with the quantum conductance G_0. Assuming that only one parabolic subband is occupied, the density of modes for 1D, 2D, and 3D conductors is defined by counting the number of confined subbands that can fit within the energy above the conduction band, and they are

$$M_{1D} = H(E - \varepsilon_1) \tag{14a}$$

$$M_{3D} = A\frac{m^*}{2\pi\hbar^2}(E - E_C) \tag{14b}$$

where H is the unit step function, ε_1 is the bottom of the first subband, m^* is the electron effective mass, and E_C is the conduction band edge. Because the density of modes is counting modes in transverse directions, the number of conducting channels in 3D bulk conductor, M_{3D}, is proportional to its cross-sectional area (A), and M_{2D} is proportional to its width (W) [9].

2.2.4 Phonon dispersion calculation

The phonon dispersion relation provides very crucial information in crystals with primitive basis atoms. With a given polarization direction, longitudinal and transverse modes are developed for both the acoustic and optical branches, and there are total of three times the number of atoms in the primitive cell: three of acoustical branches and the rest of optical branches [7]. For silicon,

therefore, three branches exist for each acoustic and transverse mode, and those branches consist of one longitudinal and two transverse modes.

The phonon dispersion relation of silicon can be obtained using lattice dynamics with correct setup of the force constants under harmonic approximation. The valence force field (VFF) method of crystal lattice dynamics technique, which is a classical atomistic force field model, has been used for the calculations. The VFF method takes into account several force field interactions such as bond stretching, bond bending, torsion and inversion interactions, and potential and force expressions for each interaction are shown in Table 1.

Those interaction equations can be adapted to the entire crystal system by applying the interatomic potential energy in terms of the position of atoms [7]. Defining the displacement of the atom from its equilibrium position, the Taylor expanded potential energy around its minimum equilibrium value can be expressed as

$$V = V_{EQ} + \frac{1}{2}\sum_k \sum_j \frac{\partial^2 V}{\partial u(R_j)\partial u(R_k)} u(R_j) u(R_k) + \cdots \qquad (15)$$

Potential energy varies quadratically with the displacements of the atoms from their equilibrium positions. For silicon which is classified under the diamond crystal structure, the potential energy needs to be modified for diatomic basis, and the dynamical matrix should be set up carefully taking care of nearest-neighbor interactions, diatomic atom interactions, and the force constants between atoms. Once the matrix has been set, solving the dynamic equation, $M\omega^2 u(R) = D\, u(R)$, for ω^2 simply produces an eigenvalue problem for a range of wavevectors. There are many approaches such as adiabatic bond charge model, DFT, and linear response theory that generate phonon dispersion relations considering not only the atomic potential but also other

related crystal structures, but the lattice dynamics approach also estimates good enough acoustic phonon dispersion relations within first Brillouin zone.

3. Thermoelectric Properties of 3D and 1D Systems

3.1 Seebeck Coefficient

The Seebeck coefficient S and the electrical conductance G can be obtained for all dimensions using the derived equations above, Eqs. (10) and (11). Parameters that need to be considered with different dimensions are the number of conducting channels and the energy levels of the first subbands because they vary with dimension. In Fig. 3, S, G, and the power factors S^2G are compared across dimensions assuming ballistic conductors with $\Im(\mathcal{E}) = 1$, and an independent variable is $\eta_F = (E_F - \varepsilon_1)/k_BT$, to see the behaviors of the properties with the position of Fermi energy level, E_F.

Although the magnitude of S in 3D is greater in 3D than in 1D, they cannot be compared at the same η_F. Because their lowest subband energies are different, they are not under the same conditions at the same η_F. More importantly, the power factor S^2G should be considered to see the improvement of ZT [10]. However, concerning the units of G in 3D containing an area term in addition to that of G_{1D}, it is impossible to directly compare S^2G_{3D} values with S^2G_{1D} values. To make the power factors comparable to each other, they need to be normalized with their own effective density of modes defined by $M_{eff} = \int M(E)\left(-\frac{\partial f_0}{\partial E}\right)dE$, and the power factors per mode S^2G/M_{eff} for each dimension are established in Table 2. The maximum S^2G/M_{eff} increases in 1D over 3D which implies that the modes are more effectively used in 1D than in 3D.

3.2 Lattice Thermal Conductivity

Lattice thermal conductivity of a solid is defined with respect to the steady-state flow of heat along a conductor with a temperature gradient, $j_U = -\kappa\, dT/dx$, where j_U is the flux of thermal energy. From elementary kinetic theory, the thermal conductivity is expressed by Debye [7] as $\kappa_l = \frac{1}{3} C v \ell$, with C as the heat capacity per unit volume, v the average phonon velocity, and ℓ the phonon mean free path. The heat capacity from the Debye model can be defined with the relaxation time approximation as [12]

$$C = \frac{3V\hbar^2}{2\pi^2 v^3 k_B T^2} \int_0^{\omega_D} d\omega \; \frac{\omega^4 e^{\hbar\omega/k_B T}}{\left(e^{\hbar\omega/k_B T}\right)^2} = 9k_B \left(\frac{N}{V}\right)\left(\frac{T}{\theta_D}\right)^3 \int_0^{\frac{\theta_D}{T}} \frac{x^4 e^x dx}{(e^x - 1)^2} \qquad (16)$$

where k_B is Boltzmann's constant, θ_D is Debye temperature, V is the unit volume, ω is phonon frequency, and $x = \frac{\hbar\omega}{k_B T}$. At low temperatures, acoustic phonons are normally excited, so the Debye model is more appropriate for approximating the heat capacity. However, it is not valid for phonons with high frequencies because the Debye model assumes a linear dispersion, which is not around the boundary of the first Brillouin zone and is therefore completely wrong for optical phonons. More appropriate at higher temperatures and higher frequencies is the Einstein model, which assumes that all phonons have the same frequency. Although electrons also contribute to the specific heat, this contribution is typically much smaller than the phonon heat capacity and so has little effect on the total thermal conductivity.

In [13], the Debye model calculating the lattice thermal conductivity has been modified by assuming that the phonon scattering processes can be represented by relaxation times which are functions of frequency and temperature with the Planck distribution function. The model deals with boundary scattering, normal three-phonon processes, isotope scattering, and umklapp

scattering, and the normal process has a comparably small effect on the thermal conductivity at low temperatures [13]. The lattice thermal conductivity interpreted using Callaway's formalism looks like [14]

$$\kappa_{l,Bulk} = \frac{k_B}{2\pi^2 v}\left(\frac{k_B T}{\hbar}\right)^3 \int_0^{\frac{\theta_D}{T}} \tau_C(x,T)\frac{x^4 e^x dx}{(e^x-1)^2} \quad (17)$$

where τ_C is a combined relaxation time which is thus taken as $\tau_C^{-1} = \tau_B^{-1} + \tau_I^{-1} + \tau_U^{-1}$, where the right-hand-side terms are relaxation times for boundary, isotope, and umklapp scattering of the phonons, respectively. The result of the calculation for silicon is shown in Fig. 4(a) with the experimental data by Glassbrenner.

Considering an enhancement of ZT, a decrease in thermal conductivity is a significant issue in designing new devices. It has been known that the lattice thermal conductivity of semiconductor nanostructures depends on dimensions when the mean free path of carriers is comparable to the device dimensions [15]. For the case of nanowires, the phonon boundary scattering is expected to be the most dominant scattering mechanism. This can be confirmed by comparing the phonon mean free path of nanowires with varying width or diameter of the cross section [16]. In this regard, the lattice thermal conductivity for nanowires has to take spatial confinement into account, and the equation for $\kappa_{l,NW}$ can be derived by modifying the relaxation term in Eq. (17) [15].

$$\kappa_{l,NW} = \frac{k_B}{2\pi^2}\left(\frac{k_B T}{\hbar}\right)^3 \int_0^{\frac{\theta_D}{T}} \frac{\tau_C(x,T)}{\langle v\rangle} S[\gamma(x),\epsilon]\frac{x^4 e^x dx}{(e^x-1)^2} \quad (18)$$

where $\gamma(x) = [w/\Lambda(x)]$ is the reduced side length of a square cross section, w is the width of the cross section, $\Lambda(x)$ is the phonon mean free path, $\langle v\rangle$ is the averaged phonon group velocity, and S is a complicated function related to the boundary scattering with ϵ the fraction of scattered carriers at the boundary. The averaged group velocity $\langle v\rangle$ is determined by the functional

dependence of the phonon group velocity on phonon energy. Using dispersion relations for confined phonons in nanowires, the averaged group velocity is calculated over all contributing branches [17]. Figure 4(b) shows the lattice thermal conductivities of silicon nanowires with varying width. Compared to the lattice thermal conductivity of bulk silicon, the nanowires show significant decreases in thermal conductivity, and a decrease in $\kappa_{l,NW}$ with reduced width w because of a decrease in relaxation time τ_C caused by significantly increasing the boundary scattering.

3.3 Enhancement of ZT in 1D System

Based on the above calculations of the power factors and the thermal conductivities of bulk and nano-scaled silicon, the thermoelectric figure of merits can be obtained. First it is necessary to compute all the properties for the same independent variable, and Fig. 5 regenerates the Seebeck coefficients and the power factors per mode in 3D and 1D with varying temperatures. Unlike the plot of S versus η_F in Fig. 3(a), the temperature dependent S in 1D is obviously greater than S in 3D, and so is the temperature dependent S^2G per mode in 1D.

With the lattice thermal conductivities calculated in the previous section, ZT in 3D and 1D are calculated. Because the electrical conductance G used in this calculation has already been normalized by the effective density of modes M_{eff}, it can replace the electrical conductivity σ. The temperature dependent ZT of bulk silicon and 22 nm wide nanowire investigated in this study are plotted in Fig. 6 along with other experimental and theoretical data from the published papers [2,17,19]. In the range around 300K, ZT of the 22nm nanowire varies from 0.3 to 0.43 while that of the bulk silicon is below 0.1. Although the ZT values theoretically obtained in this work seem not to match very well with the data from the previous works, the great improvement

of ZT in lower dimensional semiconductor is the remarkable feature. This enhancement mostly comes from the reduced thermal conductivity in 1D since the variation of the power factor from 3D to 1D is smaller than that of the thermal conductivity.

4. Enhanced Thermoelectric Performance

4.1 Geometry Engineering

A great enhancement of ZT in ultra-small-scale semiconductor has been reported in the foregoing. We can achieve even higher ZT through an approach called *electron-crystal, phonon-glass*. Semiconductor nanowires with nano-engineered geometries are expected to draw more efficient phonon-surface scattering as the diameter is reduced to below 50 nm [21,22]. The corresponding drop in thermal conductivity may provide an enhancement of ZT if the electronic transport is not as affected by surface scattering. Previous work by Martin [21,24] suggests the enhancement of the figure of merit through interactions of the carriers with repetitive patterns at the wire boundaries. In this work, sinusoidal wires (SineNW) are considered, as schematically depicted in Fig. 7(a), which may be candidates to realize a phonon blockade as discussed in [23] without degrading appreciably the electronic current.

4.1.1 Electronic transport

Solutions of electronic quantum transmission for silicon bars with sinusoidal undulations are shown in Fig. 7(b), including a comparison with straight bars of the same cross-section. The transmission coefficient, which represents the number of modes contributing to transmission in a straight and smooth wire, is directly proportional to the wire resistivity due to the scattering mechanism. The 3D conduction channel is modeled by a 1D tight binding chain, and the quantum nature is accounted for by solving the Schrödinger equation for each cross section in the transverse direction [6]. Different cross sections can be readily included in the model. Silicon nanowires with length of 30 nm and cross sectional width of 6 nm and 10 nm are considered, with several numbers of undulation peaks (N) and heights (H). N and H define the shape of

undulation within the fixed length (L) by changing periods of undulation. The nanowire undulations directly affect the resistivity particularly at higher carrier energy. However, for the narrower wire, one can see that increasing the number of undulations only decreases the transmission coefficient in a small way.

4.1.2 Phononic transport

The thermal conductivity of thin nanowires deviates substantially from the bulk due to phonon blockade with a presence of boundary scattering which is dominant in mesoscopic scale devices among the scattering mechanisms. To solve the problem of phonon transport through confined systems, besides BTE and molecular dynamics (MD), a transmission function approach is very well suited when phonons flow ballistically [25]. This approach enables atomistic investigation of phonon transport through 3D nanowire systems. This work requires complex harmonic matrices of each cross section of the targeted model, and the matrix setup procedure will be discussed in the following section. Harmonic matrices for the system of interest and its components to establish the harmonic relationship between any two atomic degrees of freedom should be obtained with equilibrium atomic positions and a prescribed interatomic potential energy model. Then, the Green's function of the system is calculated from the pre-defined harmonic matrices [26]. Thereafter, the net heat flow rate can be calculated from integration over the full frequency spectrum for specified contact temperatures. Since the atomic scale system is treated using Green's function method, it is also called the Atomistic Green's Function (AGF) method [25-28]. After setting up the harmonic matrices of a nanowire constructed as shown in Fig. 7 (a), the nanowire Green's function and the transmission function are expressed as

$$\mathbf{G} = (\omega^2 \mathbf{I} - \mathbf{H} - \Sigma_L^d - \Sigma_R^d)^{-1} \tag{19}$$

$$\mathrm{T}(\omega) = \mathrm{Tr}[\,\mathbf{\Gamma_L}\,\mathbf{G}\,\mathbf{\Gamma_L}\,\mathbf{G}^{\dagger}] \tag{20}$$

where H is the harmonic matrix of the nanowire and Σ_L^d and Σ_R^d are the self-energy matrices of the left and right contacts. Just like the transmission probability in the electrical conductivity equation, Eq. (10), one can obtain heat flux through a nanowire using the transmission function derived in Eq. (20). A great advantage of the AGF method is that any dimension or length of a real atomic system can be handled under harmonic assumption. Actually, the dependence of phonon transport on nanowire diameter and length was studied by Zhang et al. [27] and higher thermal conductance with increasing cross section area and decreasing length was proved as expected. This technique can be now benchmarked to see the phonon transport behavior through the undulated nanowire. Real-size 3D silicon nanowires are constructed in atomic scale with different numbers of undulation peaks and heights and used for the thermal conductance calculation. Transmission function as a function of angular frequency is shown in Fig. 8.

The sum of the transmission function of the SineNW over the whole frequency region is lower than the straight bar NW, 19.03 compared to 28.61 respectively. This result leads to the lower thermal conductance through the undulated than through the straight nanowires because heat flux through a conductor is defined as a product of transmission function and phonon distribution functions in the left and right contacts [28]. Therefore, proper geometry engineering is expected to draw the enhancement of ZT by preventing phonon transport effectively as electronic transport is not affected.

4.1.3 Harmonic matrix setup

Figure 9 shows a part of the FCC lattice structure, with a basis containing two identical atoms, which is used in the lattice dynamics technique for silicon. The atoms with solid circles belong to one FCC structure, and the atoms with the open circles are in the other.

As explained in the above chapter, the VFF method is applied to the diatomic diamond lattice structure, and the harmonic matrix discussed in the Green's function calculation can be obtained. The procedure is as follows. One has to define the interatomic potential between the nearest neighbors, up to the third nearest neighbors at least, and the dynamical matrix is generated by taking the second derivative of the potential with respect to all the displacement vectors, u_{11}, u_{12}, u_{13}, etc. Finding the set of eigenvalues of the dynamical matrix at different wave vectors produces the phonon dispersion relation of the targeted model, and the dispersion relation of silicon is displayed in Fig. 10. Solid lines are the dispersion relations with the dynamical matrix of up to 4th nearest neighbors, and the dotted lines are with up to 3rd nearest neighbors. Since only bond bending interactions of the VFF method were included in the lattice dynamics calculation, the optical mode branches are slightly off from the experimental data, but the acoustic mode branches which really affect the phonon transport through the device were accurate enough to see the phonon transmission variations.

4.2 Thermal Conductivity of Superlattice Nanowires (SLNW)

It has been known that the lattice thermal conductivity of semiconductor nanowires depends on dimensions when the mean free path of carriers is comparable to the device dimensions. In addition to the predominant boundary scattering mechanism in a pure semiconductor nanowire, interface scattering in between two different types of semiconductor segments poses significant resistance to phonon transport in superlattice nanowires [29].

Because it is well known that the phonon density of states is dominated by acoustic phonon modes at low temperature, especially lower than Debye temperature, in this work longitudinal

acoustic (LA) and transverse acoustic (TA) phonons are considered as heat transport media. While the Debye approximation assumes that the longitudinal and transverse polarization behave identically for the simplicity, a more accurate result can be achieved when the heat capacity and the sound velocity are treated as function of phonon frequency that can be defined using each LA and TA phonon dispersion relation. To achieve an improvement of accuracy by adopting these concepts, the heat capacity equation should be modified treating the phonon polarization independently and using the phonon group velocity dependent on the phonon frequency. Instead of the heat capacity equation in Eq. (16), the frequency-dependent heat capacity for LA and TA phonon modes can be expressed as

$$C_{L,T} = \frac{V\hbar^2}{2\pi^2 k_B T^2}\int_0^{\omega_{L,T}} d\omega \frac{\omega^4 e^{\hbar\omega/k_B T}}{v_{L,T}{}^3 (e^{\hbar\omega/k_B T})^2} \tag{21}$$

where $\omega_{L,T}$ and $v_{L,T}$ are LA or TA phonon cutoff frequency and group velocity, respectively. In the same manner, the phonon mean free path ℓ expressed as a product of the phonon relaxation time τ and the group velocity v can be defined independently for each LA and TA phonon mode. The combined relaxation time τ_C can be obtained in terms of the scattering rates of several scattering mechanisms [14].

$$\tau_C^{-1} = \tau_B^{-1} + \tau_I^{-1} + \tau_U^{-1} \tag{22}$$

where τ_B, τ_I, and τ_U are the relaxation times for boundary, isotope, and umklapp scattering of the phonons.

$$\tau_B{}^{-1} = \frac{v}{L} \tag{23}$$

$$\tau_I{}^{-1} = \frac{3V_0\Gamma\omega^4}{\pi v^3} \tag{24}$$

$$\tau_U{}^{-1} = \frac{h\gamma^2}{2\pi m\theta\, v^2} \exp\left(\frac{-\theta}{3T}\right) \omega^2 T \quad (25)$$

All the parameters used in the above three scattering rate calculations for silicon and germanium are summarized in Table 3 [14]. The frequency dependent group velocity is directly obtained from the phonon dispersion relations of silicon and germanium generated by the VFF lattice dynamics approach. It is a reverse process of finding group velocity at a certain wavevector: Finding a wavevector corresponding to the frequency needed in the calculation and calculating the slope of the acoustic phonon mode branch at the wavevector. Replacing the phonon mean free path term with the phonon group velocity and the relaxation time enables us to express all the components in the lattice thermal conductivity as function of the phonon frequency for each LA and TA phonon mode. The resulting thermal conductivities of bulk silicon and germanium are shown in Fig. 11.

Once the lattice thermal conductivity of bulk materials composing a superlattice nanowire are obtained, the thermal conductivity for the superlattice nanowire can be modeled based on the phonon Boltzmann transport equation with diffuse mismatch interface conditions [29]. When the wire diameter and the segment length become smaller than the bulk phonon mean free path, the superlattice nanowire thermal conductivity is defined by effective thermal conductivity of composed bulk materials, and the effective thermal conductivity is obtained by a ratio of the corresponding effective phonon mean free path to the bulk phonon mean free path.

$$l_{A,eff}{}^{-1} = l_A{}^{-1} + \frac{4}{3} L_A{}^{-1} + \frac{1}{\alpha_A} d_w{}^{-1} \quad (26)$$

$$\kappa_{A,eff} = \left(\frac{l_{A,eff}}{l_A}\right) \kappa_A \quad (27)$$

$$\frac{L}{\kappa_{SL}} = \frac{L_A}{\kappa_{A,eff}} + \frac{L_B}{\kappa_{B,eff}} \quad (28)$$

The above three equations are the effective phonon mean free path, the effective thermal conductivity of one of the composing materials, and the final thermal conductivity for the superlattice nanowire, respectively, where L_A, L_B are segment lengths, d_w is a wire diameter, and α_A, α_B are geometric factors which are set to be 1 in this work [29]. Equation (26) implies effective phonon-scattering length of $3L_A/4$ and $\alpha_A d_w$ for interface and wire boundary scattering, and thus the segment length and the wire dimensions are the critical factors that limit phonon transport through the system.

Figure 12 (a) compares the thermal conductivity of Si/Ge superlattice nanowires with the experimental thermal conductivity data of Si/SiGe superlattice nanowires from [18]. For two different diameters, 58 and 83 nm, the thermal conductivities estimated in this study are slightly higher than the experimental data, but they are pretty close to each other considering that the model used in the experiment is Si/SiGe with Ge concentration of 5 to 10 %. Figure 12 (b) shows temperature dependent thermal conductivity of Si/Ge superlattice nanowires, and they do not vary much with temperature.

Figure 13 shows a dependence of the thermal conductivity on diameters at 300 K, and decreasing diameters have a detrimental effect on the thermal conductivity. In addition, the thermal conductivity changes more drastically in a diameter regime below 50 nm, while it shows even more constant behavior with segment length less than 30 nm in the opposite regime.

Figure 14 displays the segment length dependent thermal conductivity of superlattice nanowires at 300 K with varying diameters. Like the thermal conductivity behaviors with varying diameter, thermal conductivity with varying segment length is observed to decrease with segment length less than 50 nm, as shown in Fig. 14. Careful examination of the reductions of the thermal

conductivity with the decreasing segment length and dimension shows that the segment length variation has a more significant impact than the diameter variation. This proves that the resistance due to the interface scattering is dominant over that due to the boundary scattering, and that should explain how significant reduction of thermal conductivity can be achieved using superlattice structures out of pure semiconductor structures.

5. Conclusion

Thermoelectric properties of bulk (3D) silicon and nanowires (1D) were investigated in this study. Enhancement of the thermoelectric figure of merit ZT in a low-dimensional system has been addressed by reducing thermal conductivity due to an increase in boundary scattering mechanism. The Landauer approach with ballistic assumption has been taken to the calculation of the Seebeck coefficient and electrical conductivity, and normalized Seebeck coefficient and power factor slightly improved in the 1D system which contributed to the enhancement of ZT. The lattice thermal conductivity was calculated from the phonon Boltzmann transport equation in the relaxation time approximation, and reduced thermal conductivity with decreasing cross-section dimensions of nanowires has been confirmed. At the end of the comparison between 3D and 1D systems, theoretically calculated ZT in 1D became a few orders of magnitude greater than that in 3D, showing that silicon nanowires are candidates for future thermoelectric applications. To achieve even higher ZT, thermoelectric properties of sinusoidally undulated nanowires were investigated and resulted in a reduction of lattice thermal conductivity without much degradation on electronic transport. In addition to the geometry engineering, thermal conductivity of Si/Ge superlattice nanowires was calculated adopting the frequency dependent thermal conductivity calculation technique, and the SLNW has proposed itself as a potential candidate for the thermoelectric engineering structure. Based on the results in this work, other applicable materials and geometries can be proposed later to test their thermoelectric performance.

6. Figures

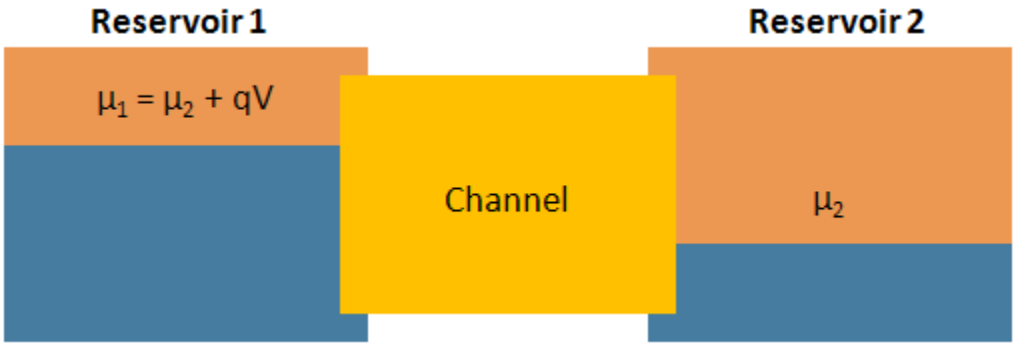

Figure 1 A single channel between two reservoirs for an applied bias voltage difference V_1-V_2. The terms $\boldsymbol{\mu_1}$ and $\boldsymbol{\mu_2}$ are the chemical potentials on the left- and right-hand sides, respectively, and $\mathbf{q} = -\mathbf{e}$ for electrons and $+\mathbf{e}$ for holes.

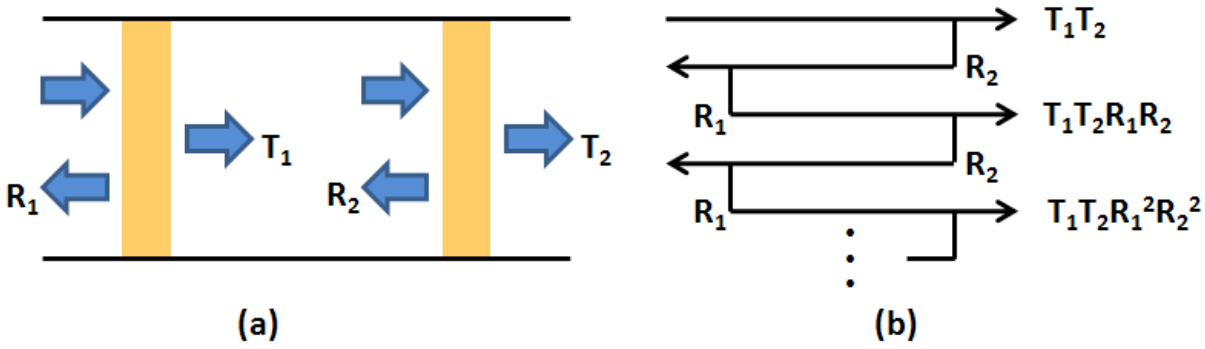

Figure 2 (a) Two resistors connected in series with transmission probabilities T1 and T2 and reflection probabilities R1 and R2. (b) The net transmission through two scatterers by summing the probabilities of all reflected paths.

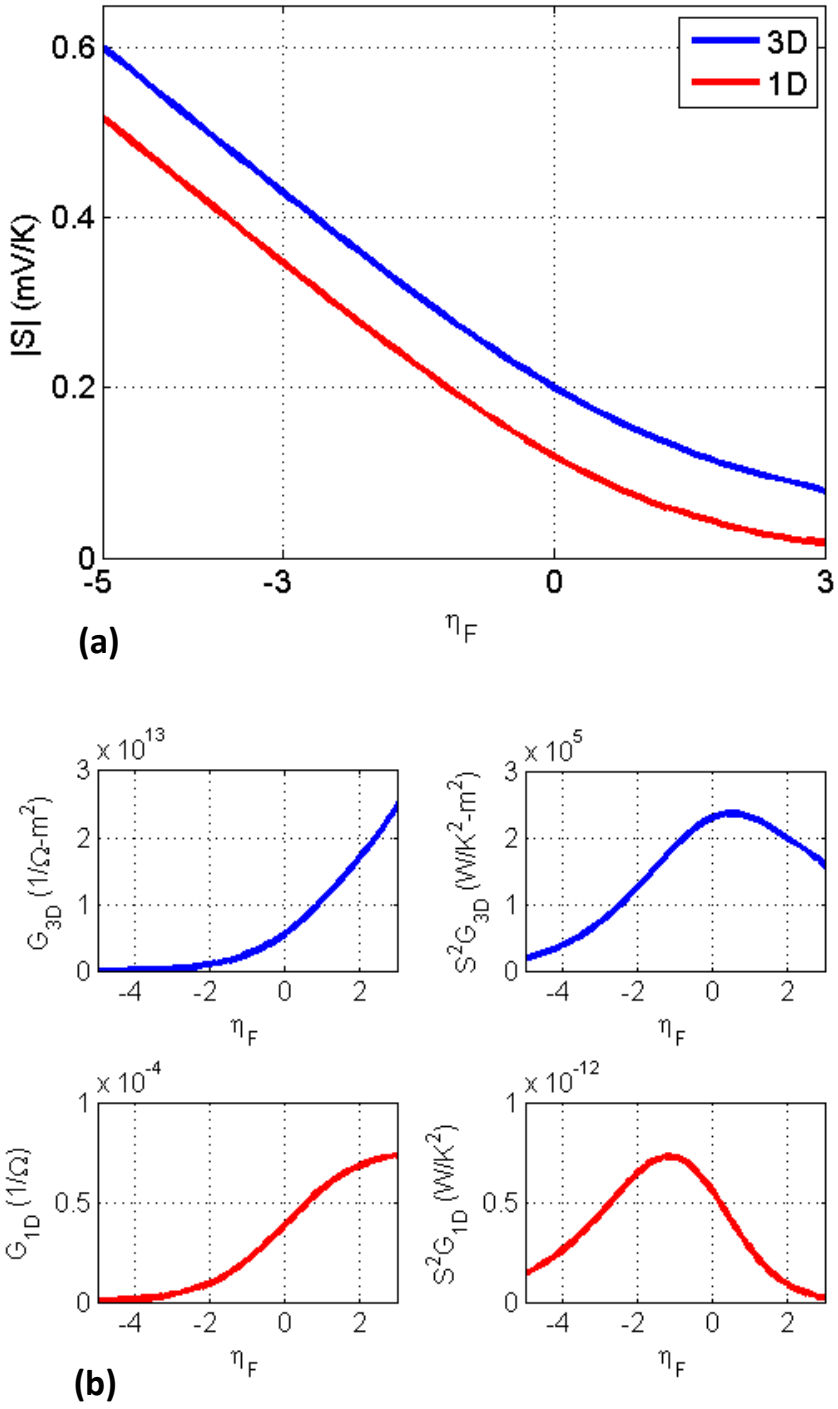

Figure 3 Model calculation results for (a) the Seebeck coefficients, (b) the electrical conductance and power factors in 3D and 1D, T = 300K and m* = m_0.

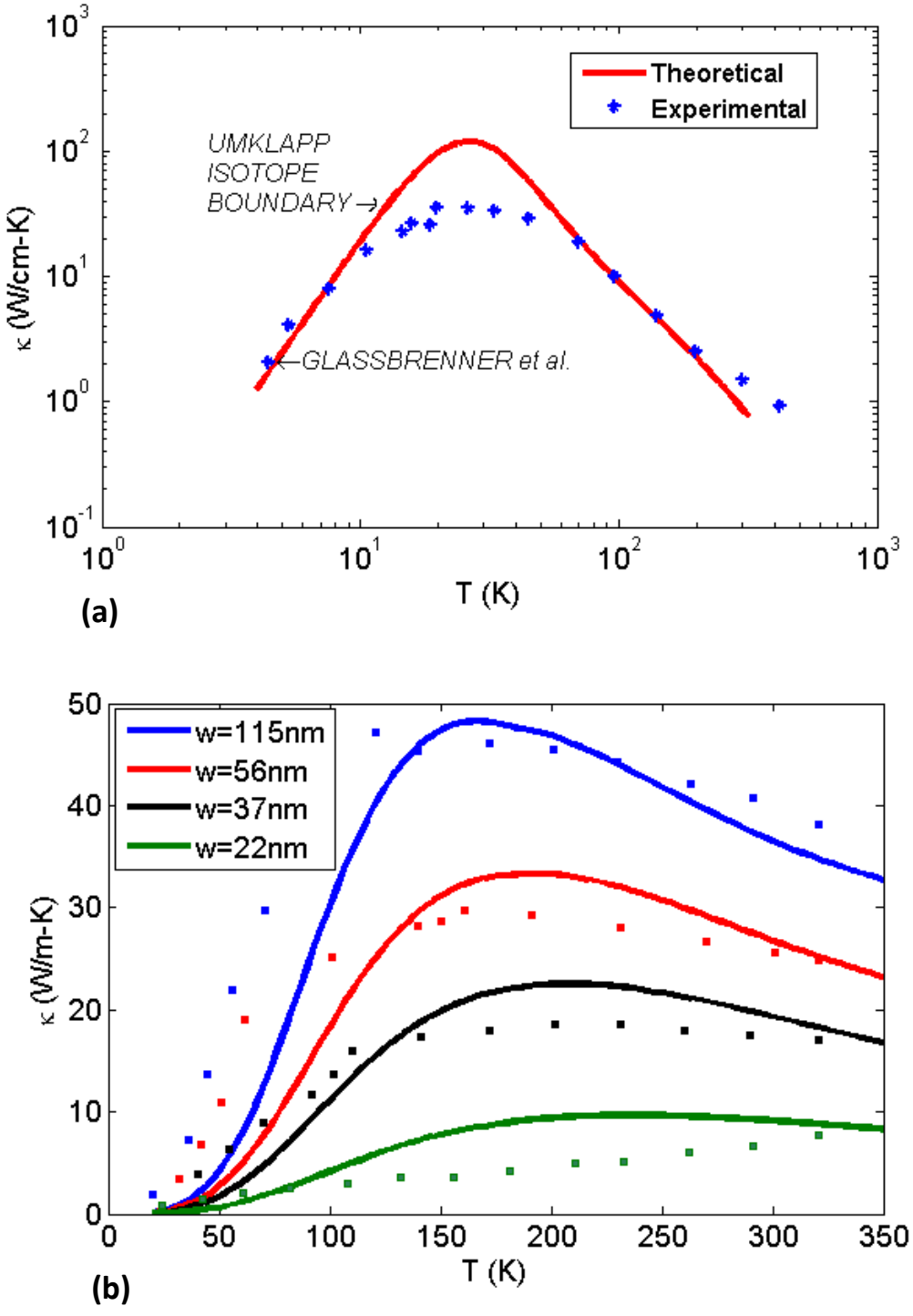

Figure 4 Comparison of the low-temperature κ results for bulk Si with $v = 9.5\times10^5$ cm/s and $\theta = 674$ K. (b) Thermal conductivities of nanowires with varying width. Solid lines are theoretical values calculated in this study, and squares are experimental data taken from [18].

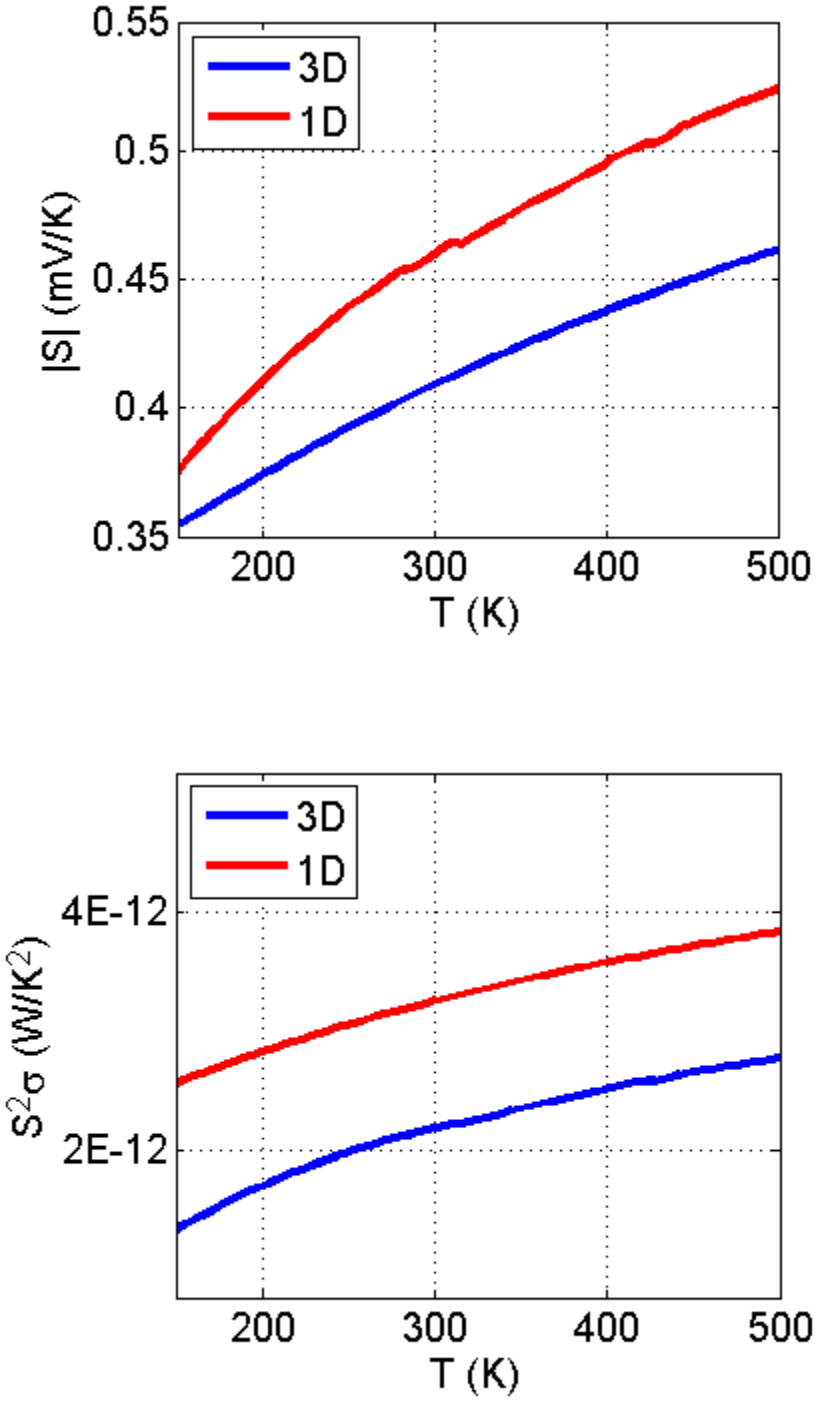

Figure 5 $\boldsymbol{S}$ and $\boldsymbol{S^2\sigma}$ through 3D and 1D conductors with varying temperature.

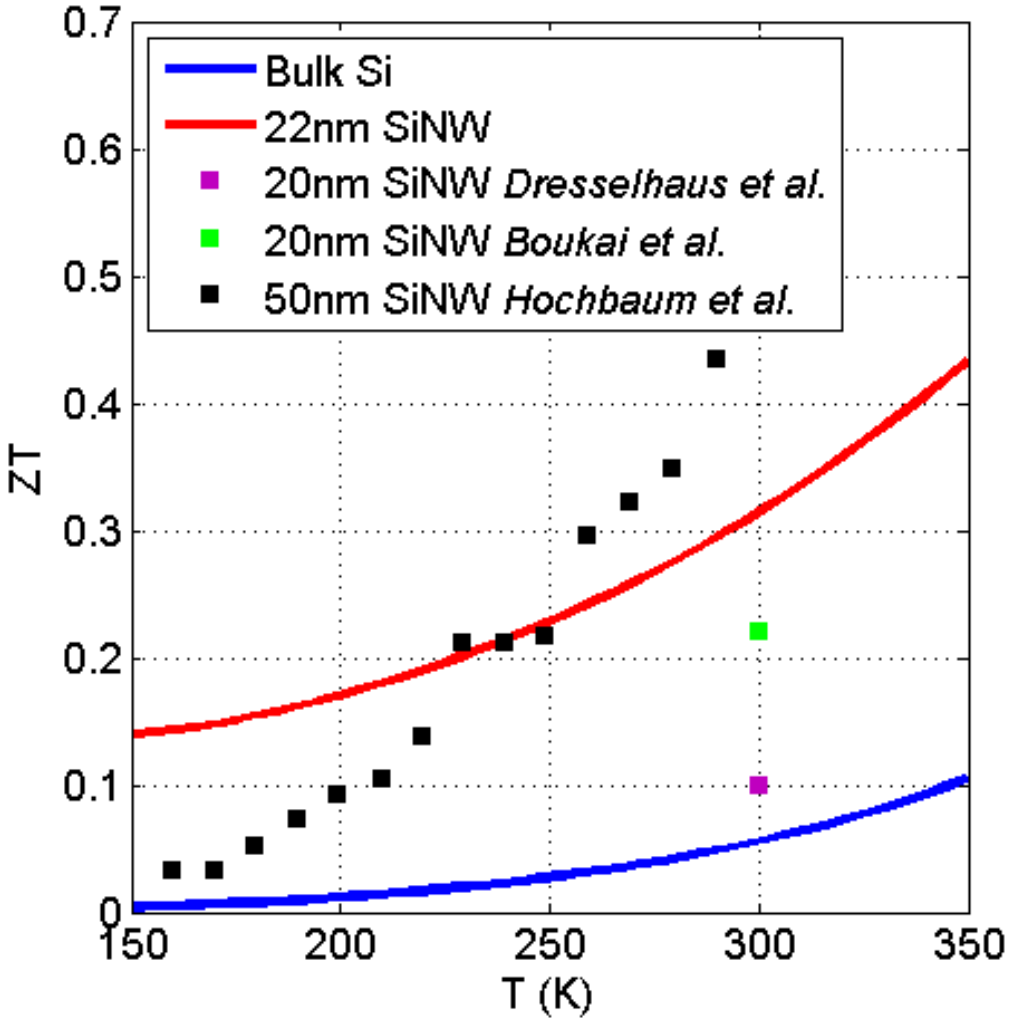

Figure 6 ZT of bulk Si and 22nm SiNW investigated in this study and data from the published papers.

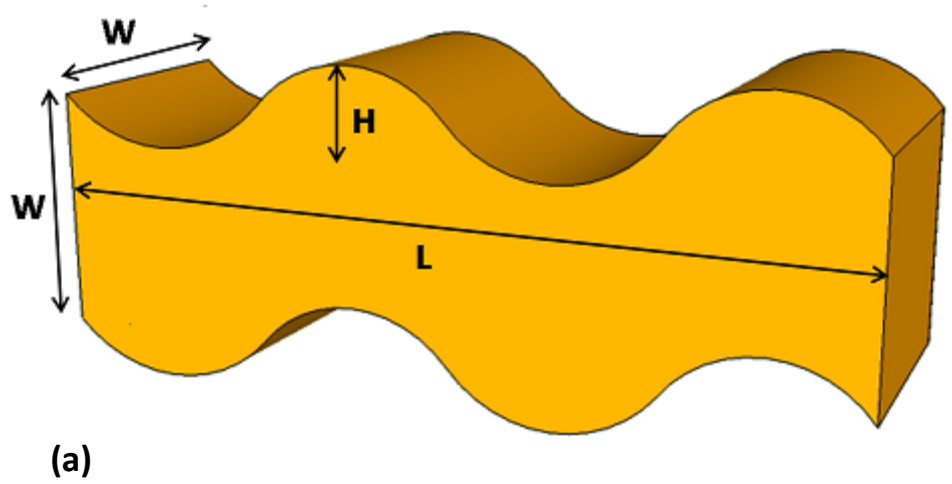

(a)

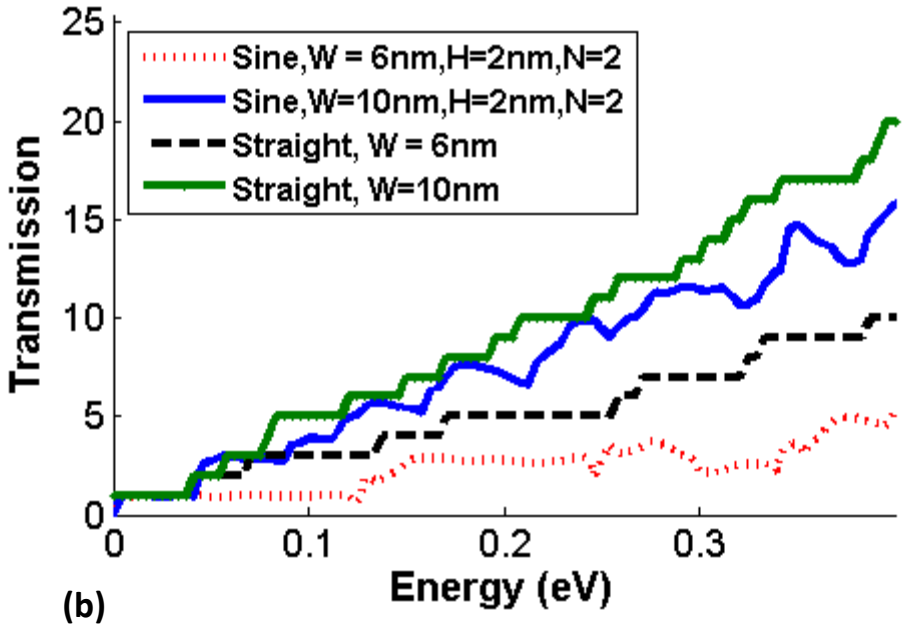

(b)

Figure 7 (a) 3D Model of a silicon nanowire with sinusoidal undulation. (b) Comparison of sine-curved NWs with straight NWs, W=6, 10nm.

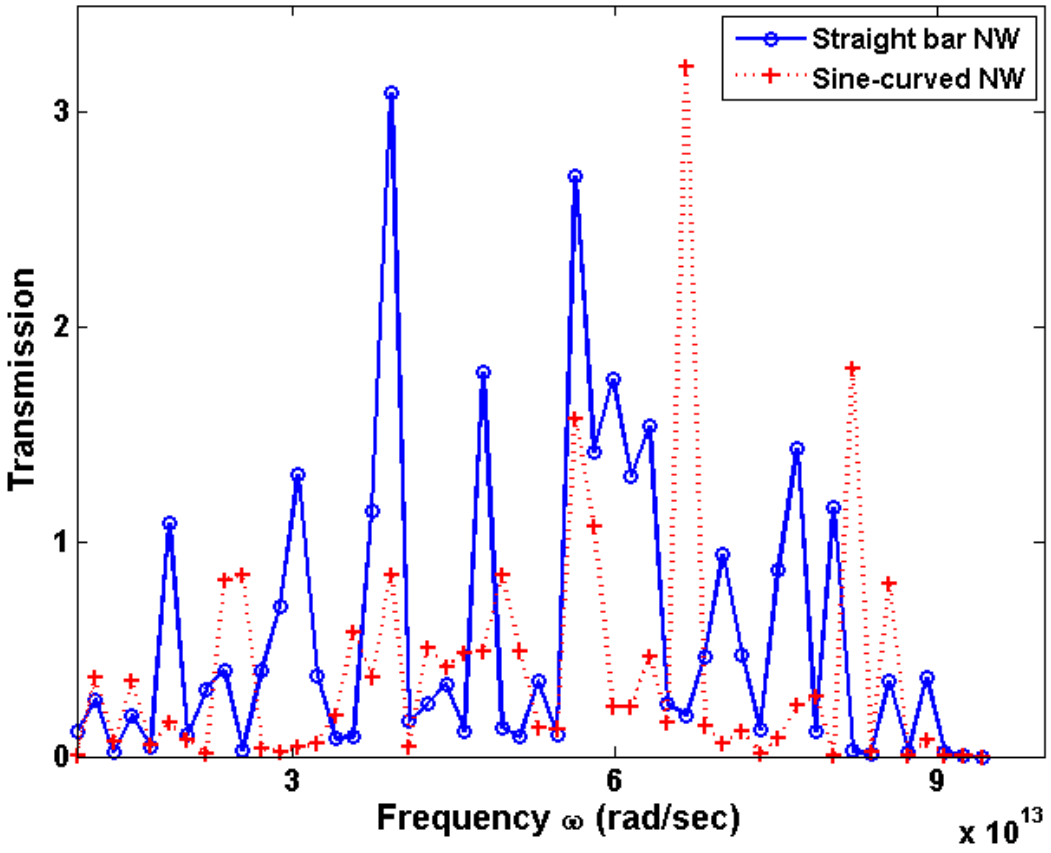

Figure 8 Comparison of transmission functions of silicon nanowire with straight and sinusoidally undulated silicon nanowires. Number of undulation peaks (N) = 2, height (H) = 2nm.

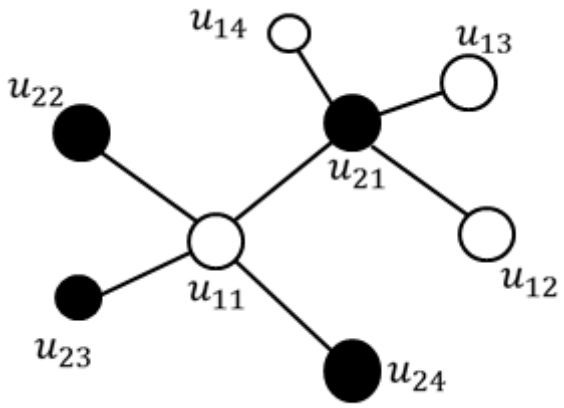

Figure 9 A part of the diatomic diamond lattice structure.

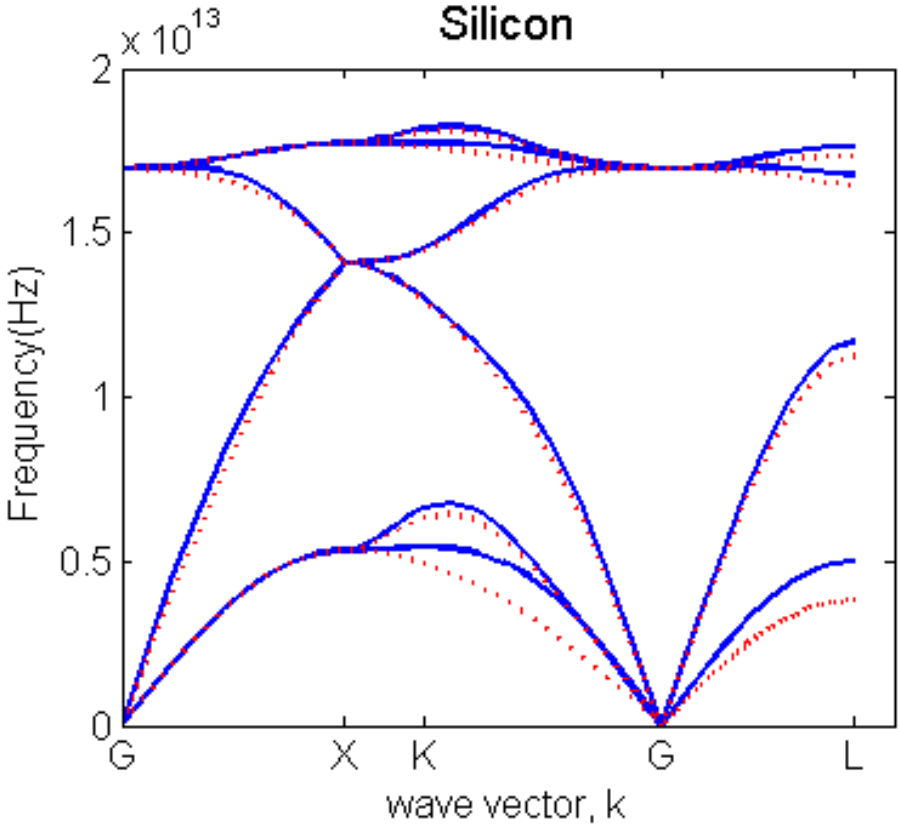

Figure 10 Phonon dispersion relation of silicon (solid line = 4th nearest neighbors, dotted line = 3rd nearest neighbors).

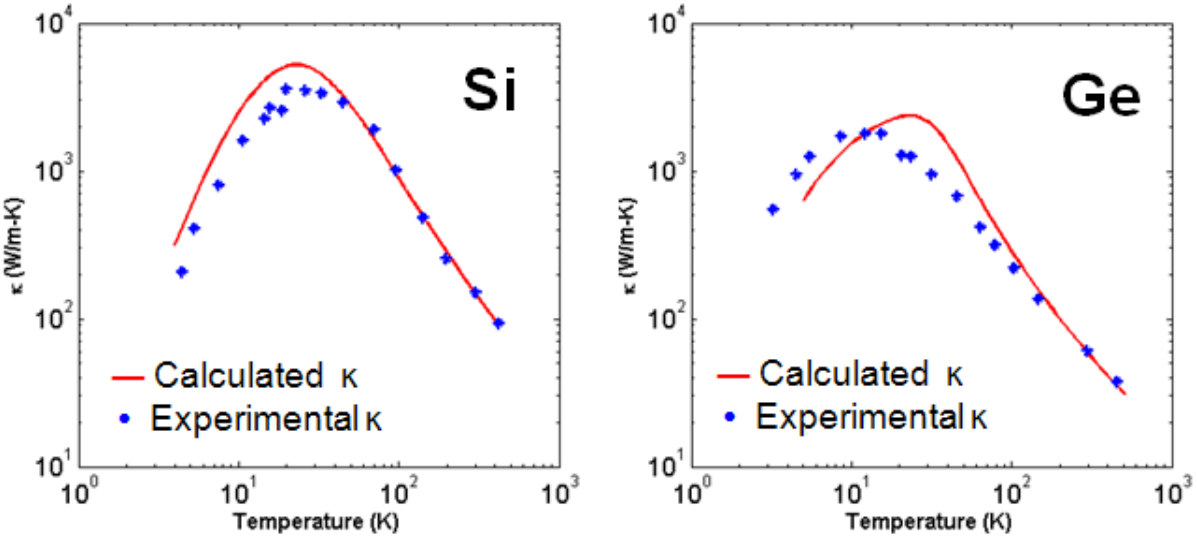

Figure 11 Lattice thermal conductivity of bulk silicon and germanium.

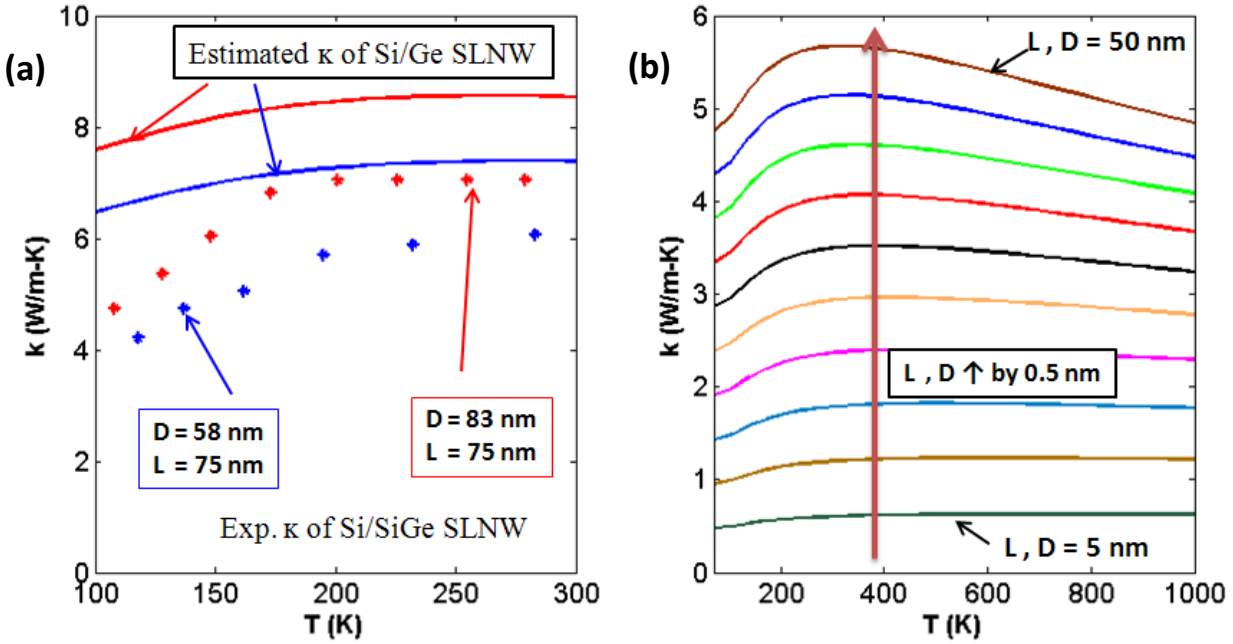

Figure 12 (a) Thermal conductivity of Si/Ge superlattice nanowires. (b) Temperature dependent thermal conductivity of SLNW.

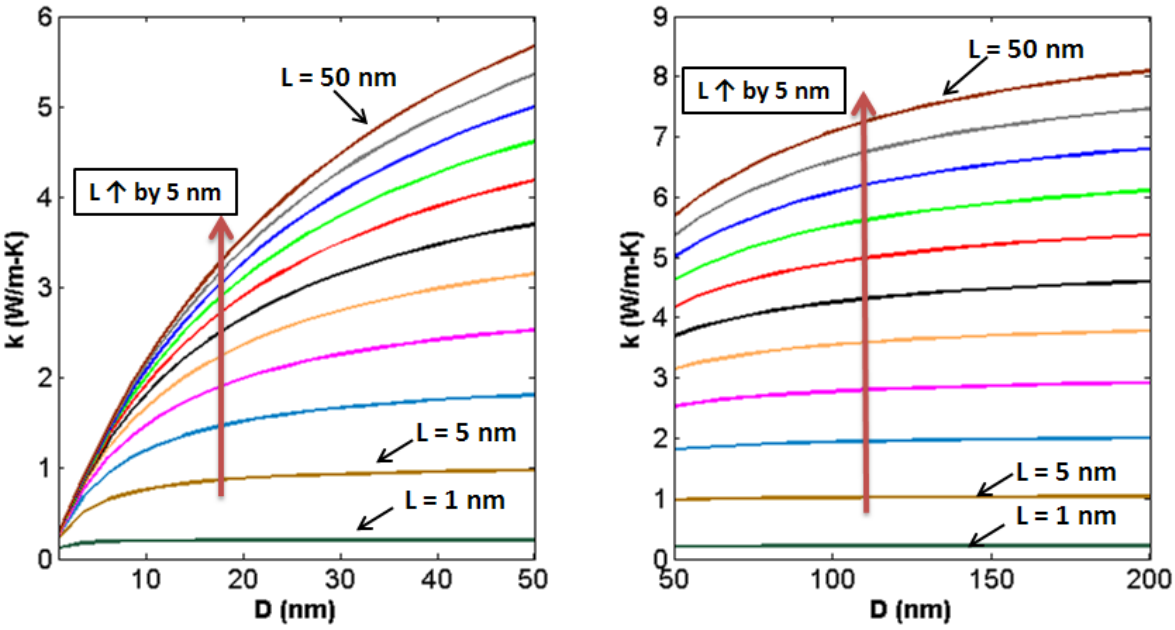

Figure 13 Thermal conductivity of Si/Ge superlattice nanowires with varying diameter at 300K.

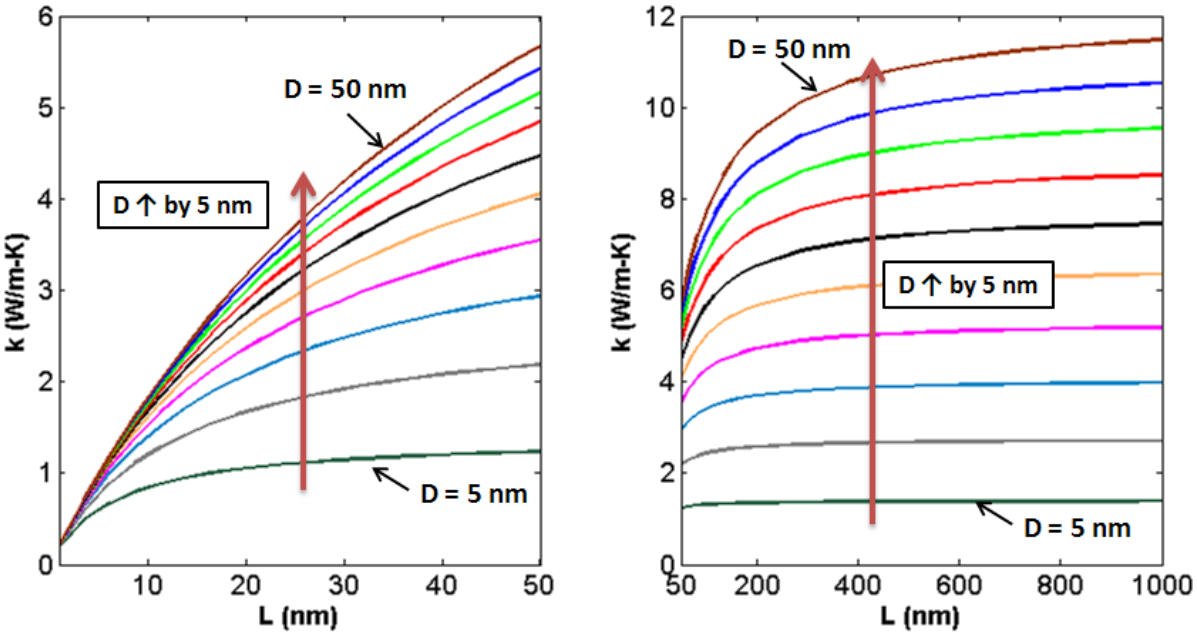

Figure 14 Thermal conductivity of Si/Ge superlattice nanowires with varying segment length at 300K.

7. Tables

Table 1 Valence force field interaction expressions

Description	Potential	Forces
Bond stretching	$U_r = \frac{1}{2}K_b(R - R_0)^2$	$-\frac{\partial U}{\partial R} = K_b(R - R_0)$
Bond bending	$U_\theta = \frac{1}{2}C(cos\theta - cos\theta_0)^2$	$-\frac{\partial U}{\partial \theta} = C(cos\theta - cos\theta_0)sin\theta$
Torsion	$U_\phi = \sum_{n=1}^{p}\frac{1}{2}K_{\theta,n}[1 - d\cos(n\phi)]$	$-\frac{\partial U}{\partial \phi} = \frac{1}{2}K_\theta dnsin(n\theta)$
Inversion	$U_\psi = \frac{1}{2}C(cos\psi - cos\psi_0)^2$	$-\frac{\partial U}{\partial \psi} = C(cos\psi - cos\psi_0)sin\psi$

Table 2 Data for the calculations of the power factor per mode for 3D and 1D

	$(\boldsymbol{S^2G})_{max.}$	$\boldsymbol{\eta_F}$	$\boldsymbol{M_{eff}}$	$\boldsymbol{S^2G/M_{eff}}$
3D	2.374×10^{5} [W/K^2-m^2]	0.519	1.045×10^{17}[m^{-2}]	2.2718×10^{-12}[W/K^2]
1D	7.270×10^{-13} [W/K^2]	-1.094	0.2509 [-]	2.8976×10^{-12}[W/K^2]

Table 3 Parameters used in the scattering rate calculations for silicon and germanium

Parameters		Silicon	Germanium
L	average diameter of the crystal	0.44 cm	0.44 cm
V_0	average volume per atom in the crystal	1.99×10^{23} cm^3	2.26×10^{23} cm^3
Γ	point impurity scattering parameter	1.65×10^{-5}	4.90×10^{-5}
γ	Gruneisen's constant	1.5	1.4
m	average mass of a single atom	28.09 g/mol	72.63 g/mol
θ	Debye temperature	674 K	395 K

References

[1] G. Chen, *Nanoscale Energy Transport and Conversion* (Oxford University Press, 2005), pp. 228-237.

[2] A. I. Hochbaum *et al*., "Enhanced Thermoelectric Performance of Rough Silicon Nanowires," Nature 451, 06381 (2008).

[3] R. K. Willardson and A. C. Beer, *Recent Trends in Thermoelectric Materials Research, Part One (Semiconductors and Semimetals) Vol. 69* (Academic Press, 2000).

[4] M. Lundstrom, *Fundamentals of Carrier Transport* (Cambridge University Press 2nd ed, 2000), pp. 191-195.

[5] D. M. Rowe, *Thermoelectrics Handbook: Macro to Nano* (Taylor & Francis Group, 2006).

[6] J. M. Ziman, *Electrons and Phonons: The Theory of Transport Phenomena in Solids* (Oxford, 1962) pp. 264-307.

[7] C. Kittel, *Introduction to Solid State Physics* (John Wiley & Sons, Inc. 8th ed, 2005).

[8] S. Datta, *Quantum Transport: Atom to Transistor* (Cambridge University Press, 2005).

[9] C. Jeong *et al*., "On Landauer vs. Boltzmann and full band vs. effective mass evaluation of thermoelectric transport coefficients," J. Appl. Phys. 107, 023707 (2010).

[10] R. Kim *et al*., "Influence of dimensionality on thermoelectric device performance," Birck and NCN Publications 539 (2009).

[11] S. Datta, *Electronic Transport in Mesoscopic Systems* (Cambridge University Press, 1st ed., 1997).

[12] G. Chen, *Nanoscale Energy Transport and Conversion* (Oxford University Press, 2005), pp. 147.

[13] J. Callaway, "Model for lattice thermal conductivity at low temperatures," Phys. Rev. 113, 1046 (1959).

[14] C. J. Glassbrenner and G. A. Slack, "Thermal conductivity of silicon and germanium from 3K to the melting point," Phys. Rev. 134, 4A (1964).

[15] X. Lu and J. Chu, "Lattice thermal conductivity in a silicon nanowire with square cross section," J. Appl. Phys. 100, 014305 (2006).

[16] M. Kazan *et al*., "Thermal conductivity of silicon bulk and nanowires: Effects of isotropic composition, phonon confinement, and surface roughness," J. Appl. Phys. 107, 083503 (2010).

[17] J. Zou and A. Balandin, "Phonon heat conduction in a semiconductor nanowire," J. Appl. Phys. 89, 5 (2001).

[18] D. Li *et al*., "Thermal conductivity of individual silicon nanowires," A. Phys. Lett. 83, 14 (2003).

[19] S. K. Bux *et al*., "Nanostructured bulk silicon as an effective thermoelectric material," Adv. Funct. Mater. 19, 2445-2452 (2009).

[20] A. I. Boukai *et al*., "Silicon nanowires as efficient thermoelectric materials," Nature 451, 06458 (2008).

[21] P. Martin *et al*., "Impact of phonon-surface roughness scattering on thermal conductivity of thin silicon nanowires," PRL 102, 125503 (2009).

[22] M. Soini *et al*., "Thermal conductivity of GaAs nanowires studied by micro-Raman spectroscopy combined with laser heating," Appl. Phys. Lett, 97, 263107 (2010).

[23] P. Martin and U. Ravaioli, "Green function treatment of electronic transport in narrow rough semiconductor conduction channels," J. Phys.: Conference Series 193, 012009 (2009).

[24] J.-S. Héron *et al*., "Phonon transport in structured silicon nanowire," available online at http://www.em2c.ecp.fr/TRN07/Heron_TRN07.pdf (2007).

[25] N. Mingo *et al*., "Phonon transport in nanowires coated with an amorphous material: An atomistic Green's function approach," Phys. Rev. B 68, 245406 (2003).

[26] P. E. Hopkins *et al*., "Extracting phonon thermal conductance across atomic junctions: Nonequilibrium Green's function approach compared to semiclassical methods," J. Appl. Phys. 106, 063503 (2009).

[27] W. Zhang *et al*., "Simulation of phonon transport across a non-polar nanowire junction using an atomistic Green's function method," Phys. Rev. B 76, 195429 (2007).

[28] W. Zhang *et al*., "The atomistic green's function method: An efficient simulation approach for nanoscale phonon transport," Heat Transfer, Part B, 51: 333-349 (2007).

[29] Y. Lin and M. S. Dresselhaus, "Thermoelectric properties of superlattice nanowires," Phys. Rev. B 68, 075304 (2003).